Improvement of breakdown characteristics of an AlGaN/GaN HEMT with a U-type gate foot for millimeter-wave power application*

Kong Xin(孔 欣), Wei Ke(魏 珂), Liu Guo-Guo(刘果果), and Liu Xin-Yu(刘新宇)†

Microwave Devices and Integrated Circuits Department, Key Laboratory of Microelectronics Device and Integrated Technology, Institute of Microelectronics, Chinese Academy of Sciences, Beijing 100029, *China*

(Received 22 March 2012; revised manuscript received 1 June 2012)

In this study, the physics-based device simulation tool Silvaco ATLAS is used to characterize the electrical properties of an AlGaN/GaN high electron mobility transistor (HEMT) with a U-type gate foot. The U-gate AlGaN/GaN HEMT mainly features a gradually changed sidewall angle, which effectively mitigates the electric field in the channel, thus obtaining enhanced off-state breakdown characteristics. At the same time, only a small additional gate capacitance and decreased gate resistance ensure excellent RF characteristics for the U-gate device. U-gate AlGaN/GaN HEMTs are feasible through adjusting the etching conditions of an inductively coupled plasma system, without introducing any extra process steps. The simulation results are confirmed by experimental measurements. These features indicate that U-gate AlGaN/GaN HEMTs might be promising candidates for use in millimeter-wave power applications.

Keywords: AlGaN/GaN HEMT, breakdown characteristics, millimeter-wave, U-type gate foot

PACS: 85.30.–z, 85.30.Tv, 73.61.Ey **DOI:** 10.1088/1674-1056/21/12/128501

1. Introduction

Wide band-gap AlGaN/GaN high electron mobility transistors (HEMTs) are promising candidates for next-generation microwave power amplifiers, owing to their large power handling capabilities.[1,2] The critical breakdown field of GaN is $\sim$ 3.3 MV/cm, about three times that of Si or GaAs. Thus, in theory, a high breakdown voltage can be realized in an AlGaN/GaN HEMT. The off-state breakdown voltage (BV_{off}) is one of the most important parameters for the device because it determines a maximum output power, $P_{max} \sim I_{max} \times BV_{off}/8$ for class A operation. Here, I_{max} is the maximum drain current. Therefore, the output power potential of AlGaN/GaN HEMT can be characterized by BV_{off}. Recently, BV_{off} of over 1 kV has been reported by several groups.[3−6] Field plate (FP) technology is a typical technique to improve the BV_{off} of a GaN-based HEMT, and HEMT with a double-FP structure was reported to supply more than 40 W/mm output power density at 4 GHz.[7] With the gate length scaled, field-plated HEMTs have been already used in millimeter-wave frequencies.[1,8,9] However, the FP structure brings about a large additional gate capacitance (C_g), which results in serious degradation of the RF characteristics, and thus leads to a reduced power gain at the operation frequency. In order to improve the breakdown performance at no significant expense to the power gain, some new device structures, such as the V-gate, slant field plate, and Y-shaped Schottky gate have been proposed and achieved good results.[10−12] Nevertheless, all these techniques will bring additional process steps and increase realizing difficulties.

In this paper, an AlGaN/GaN HEMT with a U-type gate foot (U-gate) is proposed and studied using the two-dimensional (2D) device simulation software, Atlas. A conventional T-gate device is also under investigation for comparison. The gradually changed sidewall angle of the U-gate makes it possible to effectively improve the breakdown characteristics only introducing a limited additional gate capacitance, indicating a theoretical better power performance with an inappreciable consumption of power gain. Through optimizing the inductively coupled plasma (ICP) etch-

*Project supported by the Major Program of the National Natural Science Foundation of China (Grant No. 60890191) and the National Key Basic Research Program of China (Grant No. 2010CB327503).

†Corresponding author. E-mail: xyliu@ime.ac.cn

© 2012 Chinese Physical Society and IOP Publishing Ltd

ing conditions, U-gate devices were successfully fabricated and the measurement results are consistent with the simulations. Under similar RF characteristics, the off-state breakdown of the U-gate device is greatly enhanced.

2. Device structures and simulation models

Device structures for simulation are shown in Fig. 1. It is convenient to adopt Atlas's default width of 1 μm. The epitaxial structure consists of a 0.15-μm-thick GaN buffer layer, a GaN channel layer, a 1-nm-thick AlN space layer to reduce alloy scattering,[13] a 24-nm-thick AlGaN barrier layer with Al composition of 0.25- and 120-nm-thick SiN_x passivation layer from the bottom to the top. Both of the devices have the same parameters except for the gate morphology. The detailed device parameters are listed in Table 1. Device gate length, source area width, drain area width, source-drain spacing, gate-drain spacing, gate-source spacing, and gate recess depth are respectively represented by L_g, L_d, L_s, L_{ds}, L_{gd}, L_{gs}, d_{gr}. For a submicron gate length of 160 nm, the gate recess is adopted to narrow the separation between the gate and channel, which can raise the aspect ratio, and thus suppress the short channel effects.[14,15] Air gaps are applied to both devices to minimize their parasitic capacitances.

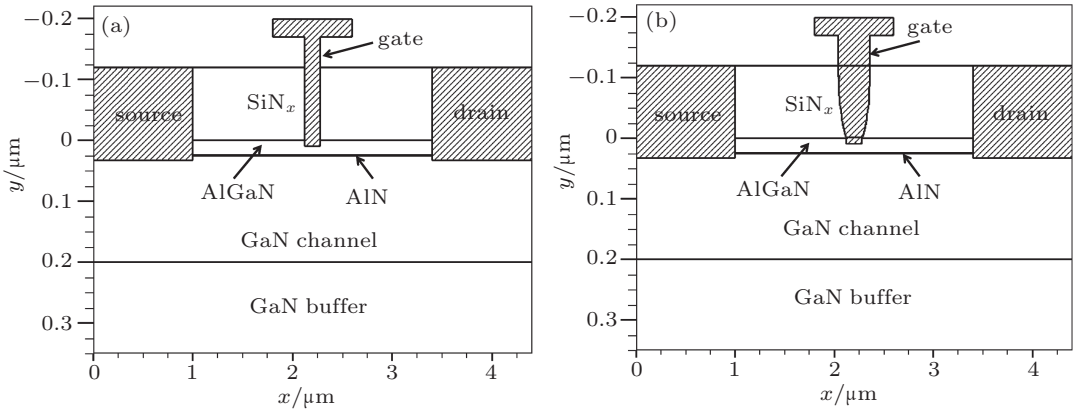


Fig. 1. (a) AlGaN/GaN HEMT with a conventional gate for simulation. (b) AlGaN/GaN HEMT with a U-gate for simulation. Both structures are coded in DevEdit.

Table 1. Geometry parameters of devices for simulation.

Structure	L_g/nm	L_d/μm	L_s/μm	L_{ds}/μm	L_{gd}/μm	L_{gs}/μm	d_{gr}/nm
T-gate	160	1	1	2.4	1.15	1.15	10
U-gate	320→160	1	1	2.4	1.04→1.12	1.04→1.12	10

In an AlGaN/GaN-based heterostructure, there exists a strong polarization effect due to the material properties of III–N compounds. The strain-induced piezoelectric polarization (P_{pi}) and the spontaneous polarization (P_{sp}) of the interface of AlGaN/GaN are taken into account in Atlas. P_{sp} can be specified on the MATERIAL statement for a given material. P_{pi} is given by

$$P_{pi} = 2\frac{a_s - a_0}{a_0}\left(E_{31} - \frac{C_{13}}{C_{33}}E_{33}\right), \qquad (1)$$

where E_{31} and E_{33} are piezoelectric constants, C_{13} and C_{33} are elastic constants, a_0 is the parameter describing the lattice constant of the material layer in question, while a_s is the parameter indicating the average value of the lattice constants of the layers directly above and below the layer in question. The specific values used for these parameters are shown in Table 2.[16] The energy band-gap, density of states, polarization effect, carrier lifetime, permittivity, effective Richardson's constant, donor, and acceptor energy levels are all critical parameters for AlGaN/GaN HEMTs' simulation and are set up in the default ma-

terial models.

Table 2. Parameters characterizing polarization effects in the AlGaN/GaN HEMT.

Parameter	Units	GaN	AlN	$Al_{0.25}Ga_{0.75}N$
P_{sp}	C/m^2	–0.029	–0.081	–0.042
a_0	Å	3.189	3.112	3.170
E_{33}	C/m^2	1.27	1.79	1.4
E_{31}	C/m^2	–0.35	–0.5	0.39
C_{13}	GPa	106	108	106.5
C_{33}	GPa	398	373	392

The GaN mobilities are assumed to be 1350 $cm^2 \cdot V^{-1} \cdot s^{-1}$ and 30 $cm^2 \cdot V^{-1} \cdot s^{-1}$ for electrons and holes, respectively. Mobilities of 100 $cm^2 \cdot V^{-1} \cdot s^{-1}$ and 5 $cm^2 \cdot V^{-1} \cdot s^{-1}$ are set in AlGaN for electrons and holes respectively. In the AlN layer, electron and hole mobility are both defined to be 100 $cm^2 \cdot V^{-1} \cdot s^{-1}$. Electron saturation velocity is set to be 1.97×10^7 cm/s while saturation velocity of the hole is assumed to be 1.0×10^6 cm/s. The sheet charge density of the positive polarization charge at the AlGaN/GaN interface is given as 1.0×10^{13} cm^{-2}. The drain and source are n-doped with a density of 1.0×10^{19} cm^{-3}, and the contact resistance is assumed to be 0.75 Ω·mm.

The drift-diffusion transport model used in this simulation is the Farahmand Modified Caughey Thomas (FMCT) mobility for a low field. The FMCT model is the result of fitting a Caughey–Thomas-like model to Monte Carlo data. For a high field, the high field-dependent mobility model is used, which is based on fitting the Monte Carlo data for bulk nitride.[17] The Shockley–Read–Hall recombination model is used to describe the generation–recombination of the carriers. Basic equations to be solved are the Poisson equation, continuity equations for electrons and holes, and transport equations using the Gummel–Newton numerical method.

The conduction band profile and electron concentration profile along the vertical direction without a gate bias are shown in Fig. 2. A quasi-triangle potential well is formed at the interface between the AlN interlayer and the GaN channel layer, and the corresponding two-dimensional electron gas (2DEG) concentration peak value is about 1×10^{20} cm^{-3}. The electron concentration declines rapidly by several orders of magnitude within tens of nanometers. These are consistent with the results from widely recognized situations in the literature,[18,19] which provides support for the reliability of these simulation models.

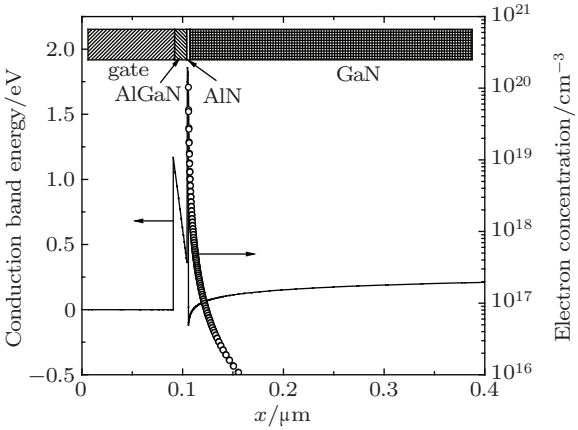


Fig. 2. Conduction band edge profile and 2DEG concentration distribution. x marks the location along the vertical direction.

3. Simulation results and discussion

3.1. Breakdown characteristics

Bahat-Treidel *et al.*[20] has reported on the simulations of AlGaN/GaN HEMT breakdown voltage. However, it is debatable whether to adopt the Albrecht low field mobility model, which is not very accurate for III–N compounds. It is generally considered that the impact ionization near the gate edge towards the drain side of the channel, where the highest electrical field region is located is a main factor which contributes to the breakdown at the pinch-off state.[21] In our simulation, in order to avoid the non-convergence problem, an electric field is simulated along the channel as an alternative to reflecting the device breakdown characteristics based on the assumption that the decrease of peak electric field (E_{pk}) is conducive to enhancing the breakdown voltage. A similar method has been utilized in Ref. [22].

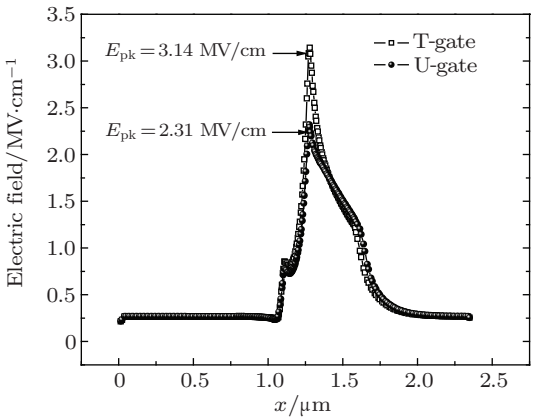


Fig. 3. Electric field distributions of both structures along the cross section in channel.

The devices are biased in the off-state with V_{gs} of -6 V and V_{ds} of 50 V. From the simulation results, we notice that the peak electric field is located at the drain side of the gate edge, which is in accordance with the results in Refs. [11] and [21]. The electric field distribution along the channel is extracted from a cutline and illustrated in Fig. 3.

The E_{pk} of the U-gate device is remarkably reduced compared to that of the conventional T-gate device (2.31 MV/cm versus 3.14 MV/cm). A lower electric field transfers less energy to electrons, thereby reducing the probability of electrons injecting into the channel from the gate electrode and subsequent impact ionization, which indicates a higher off-state breakdown voltage. Also, the U-gate device reveals a smoother electric field distribution than that of the conventional T-gate with the avoidance of a sharp decline after the peak. We believe that the U-gate device spreads out the field-crowding through the sloped gate sidewall. We account that the E_{pk} reduction of the U-gate device should be attributed to the extension of equipotential lines within the device because the distribution of equipotential lines is physically influenced by the geometrical morphology of the gate electrode. The origin of the equipotential line extension can be derived either from the gate side (U-gate device) or the gate cap (FP-gate device). For a conventional T-gate device, a similar influence from the gate cap will be interrupted and undermined by the air gap on the top of the SiN_x passivation layer. The extension of equipotential lines will lead to the re-creation of an internal electric field, and this should be the mechanism of the inhibition of the electric field in the channel. In Ref. [20], it was proposed that grating field plates could enhance the AlGaN/GaN HEMT breakdown voltage, which can also be ascribed to the extension of equipotential lines. The difference is that grating field plates provide multiple sources to extend the equipotential lines.

3.2. RF characteristics

AC simulation is performed to investigate the RF small-signal characteristics of devices with both gate structures. The gate width is changed into 75 μm. Devices are biased at $V_{gs} = -2.0$ V and $V_{ds} = +6$ V.

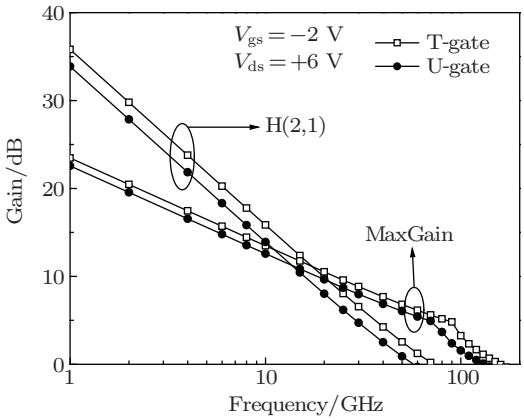


Fig. 4. Simulated RF small-signal characteristics of both structures at $V_{gs} = -2.0$ V and $V_{ds} = +6$ V.

The curves of current gain and maximum available gain of both devices are shown in Fig. 4, from which the values of f_T and f_{max} can be extracted correspondingly. According to Ref. [23], the maximum gain (G_{max}) of the device can be written as follows:

$$G_{max} \approx \frac{(f_T/f)^2}{4\left[\pi f_T C_{gd}(R_s + R_g + R_{gs} + 2\pi L_s) + G_{ds}(R_s + R_g + R_{gs} + \pi f_T L_s)\right]}, \tag{2}$$

where C_{gd}, R_s, R_g, R_{gs}, L_s, and G_{ds} represent the gate–drain capacitance, source resistance, gate resistance, gate–source resistance, source inductance, and output conductance, respectively. In addition, f_T can be expressed as

$$f_T = \frac{g_m}{2\pi\left[(C_{gs} + C_{gd})\left(1 + \dfrac{R_s + R_d}{R_{ds}}\right) + g_m C_{gd}\,(R_s + R_d)\right]}. \tag{3}$$

Assuming formula (2) to be 1, the expression of f_{max} can be derived as

$$f_{max} = \frac{f_T}{2\left[\pi f_T C_{gd}(R_s + R_g + R_{gs} + 2\pi L_s) + G_{ds}(R_s + R_g + R_{gs} + \pi f_T L_s)\right]^{1/2}}. \tag{4}$$

The frequency performance degradation of the U-gate device can be attributed mainly to the introduction of extra gate capacitance. According to formulae (3) and (4), the dependencies of $f_{\rm T}$ and $f_{\rm max}$ on $C_{\rm gd}$ are weighted higher than on $C_{\rm gs}$, especially when the short channel effects can be neglected (small output conductance). As shown in Fig. 5, $C_{\rm gd}$ only increases slightly. Though $C_{\rm gs}$ seems to display a great rise, it originates from the direct contact between the gate side and SiN_x dielectric, and the gate sidewall is gradually changed. Both are combined to make the increment insignificant as compared with the outcomes obtained using other aforementioned techniques. Moreover, the gate resistance of the U-gate device will decrease to some extent, owning to the broadening of the gate electrode. The combination of these factors induces the simulated values of $f_{\rm T}$ and $f_{\rm max}$ of the U-gate device to be 58 GHz and 135 GHz respectively, which are comparable to those of a conventional T-gate device (70 GHz and 150 GHz respectively).

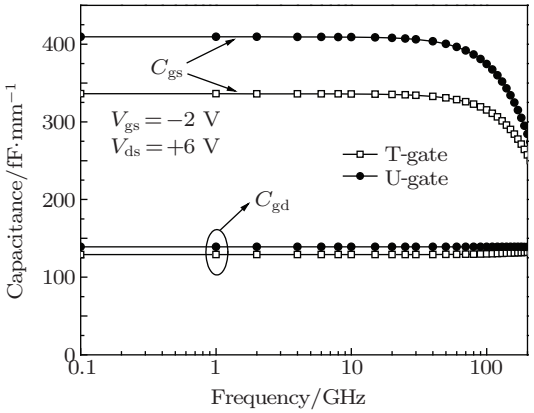


Fig. 5. Simulated curves of $C_{\rm gs}$ and $C_{\rm gd}$ versus frequency.

4. Fabrication and characterization

AlGaN/GaN HEMTs with a U-type gate foot are fabricated and characterized. The epitaxial layers are grown by metal–organic chemical vapour deposition (MOCVD) on a two-inch diameter (0001) sapphire substrate. The epitaxial layers are composed of, from the bottom, a 100-nm-thick AlN nucleation layer, a 2-μm-thick GaN buffer and channel layer, a 0.7-nm-thick AlN spacer layer, and a 22-nm-thick AlGaN barrier layer. The Al composition of the barrier layer is 21.5%, and none of the layers were intentionally doped. The fabrication steps of U-gate device are similar to those discussed in Ref. [24]. The striking difference is the delineation of gate recess by SiN_x dry etching. After etching in CHF_3 ambient for 116 s, a subsequent etching using SF_6 ambient is followed for 50 s. Through controlling the chamber pressure during the ICP etching, etching also occurs in the region beneath the overhang of photoresist. Owing to the lower etch rates in these regions, curved sidewalls are formed. The shapes of these trench walls can be controlled by varying the chamber pressure, etching time, and gas flow rate. Conventional T-gate devices are also fabricated for comparison.

Figure 6 shows the three-terminal off-state breakdown characteristics of the U-gate device and conventional T-gate device at $V_{\rm gs}$ of −8 V. The devices each feature a gate length of 160 nm, a gate width of 2×75 μm, and a source-drain separation of 2.4 μm. Here, $BV_{\rm off}$ is defined as the drain–source voltage ($V_{\rm ds}$) at which the drain current ($I_{\rm ds}$) begins to sharply increase. The $BV_{\rm off}$ of the U-gate device is about 85 V, which is 30% larger than the value of 65 V obtained in a conventional T-gate device with the same feature sizes. The physical process of off-state breakdown can be described as follows. (i) Though a high Schottky barrier exists, leakage electrons can tunnel from the gate electrode to the channel. (ii) With $V_{\rm ds}$ increasing, the impact ionization coefficient increases, resulting in an abrupt increase in the drain current triggered by the injected electrons.[25] The leakage electron tunneling and impact ionization are closely related to the electric field in the channel. The higher $BV_{\rm off}$ of the U-gate device than that of the conventional T-gate device should be ascribed to electric field alleviation in the channel.

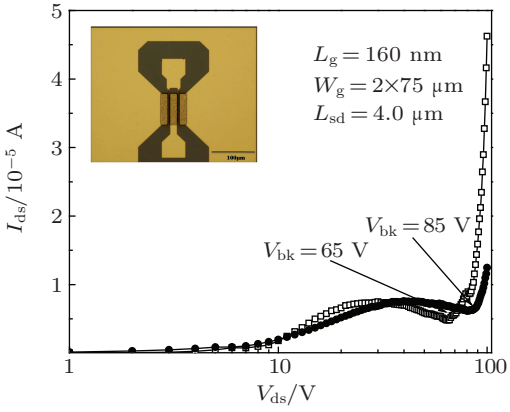


Fig. 6. (colour online) Measured three-terminal off-state breakdown characteristics of the U-gate device and conventional T-gate device at $V_{\rm gs}$ of −8 V.

The on-wafer S-parameter measurements of up to 40 GHz are carried out using an Agilent E8363B

PNA network analyzer. As shown in Fig. 7, an $f_{\rm T}$ of 65.4 GHz and an $f_{\rm max}$ of 111.6 GHz for the U-gate device are obtained at $V_{\rm gs} = -3.0$ V and $V_{\rm ds} = +6$ V by extrapolating H(2,1) and MaxGain using −20 dB/dec slope, respectively, while corresponding values for the conventional T-gate are 61.2 GHz and 115.1 GHz at $V_{\rm gs} = -2.0$ V and $V_{\rm ds} = +6$ V.

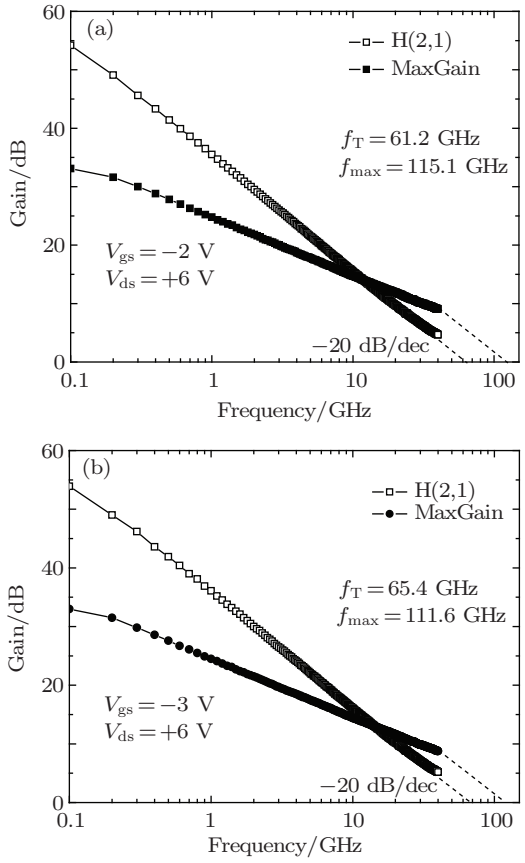


Fig. 7. (a) Current gain and maximum available gain versus frequency measured for a 160-nm conventional T-gate device with $W_{\rm g} = 2 \times 75$ μm at $V_{\rm gs} = -2.0$ V and $V_{\rm ds} = +6$ V. (b) Current gain and maximum available gain versus frequency measured for a U-gate device with the same feature size at $V_{\rm gs} = -3.0$ V and $V_{\rm ds} = +6$ V.

Except for the specific values, the simulation results fit well with the experimental measurements. The deviation of characteristics should be attributed to the limitation of carrier mobility models and material parameters for III–N compounds.

5. Conclusion

In this work, we proposed a AlGaN/GaN HEMT with a U-type gate foot for a better trade-off between the device off-state breakdown and RF characteristics. According to the 2D numerical simulation, the U-gate structure demonstrates a smoothed electric field distribution in the channel as well as a reduced $E_{\rm pk}$ due to the extension of the equipotential line. Meanwhile, with the minimized extra gate capacitance and the reduced gate resistance, the U-gate device presents comparable RF characteristics to those of the conventional T-gate device. Through optimizing the ICP etching conditions, the U-gate AlGaN/GaN HEMT has been realized and characterized. The simulation results are verified by the experimental measurements, indicating the great potential of the U-gate AlGaN/GaN HEMT for millimeter-wave power application.

Acknowledgment

The authors would like to thank all the colleagues working on GaN devices and circuits in our laboratory for fruitful discussions. We would also like to thank Li Yan-Kui and Ouyang Si-Hua for the outstanding jobs they completed during the measurements.

References

[1] Wu Y F, Moore M, Abrahamsen A, Jacob-Mitos M, Parikh P, Heikman S and Burk A 2007 *IEEE International Electron Devices Meeting*, December 10–12, 2007, Washington DC, USA, p. 405

[2] Pei Y, Chu R M, Fichtenbaum N A, Chen Z, Brown D, Shen L, Keller S, Denbaars S P and Mishra U K 2007 *Jpn. J. Appl. Phys.* Part 2 **46** L1087

[3] Dora Y, Chakraborty A, McCarthy L, Keller S, DenBaars S P and Mishra U K 2006 *IEEE Electron. Dev. Lett.* **27** 713

[4] Tipirneni N, Koudymov A, Adivarahan V, Yang J, Simin G and Khan M A 2006 *IEEE Electron. Dev. Lett.* **27** 716

[5] Uemoto Y, Shibata D, Yanagihara M, Ishida H, Matsuo H, Nagai S, Batta N, Ming L, Ueda T, Tanaka T and Ueda D 2007 *IEEE International Electron Devices Meeting*, December 10–12, 2007, Washington DC, USA, p. 861

[6] Choi Y C, Pophristic M, Peres B, Spencer M G and Eastman L F 2006 *J. Vac. Sci. Technol.* B **24** 2601

[7] Wu Y F, Moore M, Saxler A, Wisleder T and Parikh P 2006 64*th Device Research Conference*, June 26–28, 2006, Goleta, CA, USA, p. 151

[8] Palacios T, Chakraborty A, Heikman S, Keller S, DenBaars S P and Mishra U K 2006 *IEEE Electron. Dev. Lett.* **27** 13

[9] Palacios T, Chakraborty A, Rajan S, Poblenz C, Keller S, DenBaars S P, Speck J S and Mishra U K 2005 *IEEE Electron. Dev. Lett.* **26** 781

[10] Kikkawa T, Makiyama K, Imanishi K, Ohki T, Kanamura M, Okamoto N, Hara N and Joshin K 2007 *Compound Semiconductor Integrated Circuit Symposium*, October 14–17, 2007, Portland, OR, USA, p. 1

[11] Chu R M, Shen L, Fichtenbaum N, Brown D, Chen Z, Keller S, DenBaars S P and Mishra U K 2008 *IEEE Electron. Dev. Lett.* **29** 974

[12] Pei Y, Chen Z, Brown D, Keller S, Denbaars S P and Mishra U K 2009 *IEEE Electron. Dev. Lett.* **30** 328

[13] Shen L, Heikman S, Moran B, Coffie R, Zhang N Q, Buttari D, Smorchkova I P, Keller S, DenBaars S P and Mishra U K 2001 *IEEE Electron. Dev. Lett.* **22** 457

[14] Guerra D, Akis R, Marino F A, Ferry D K, Goodnick S M and Saraniti M 2010 *IEEE Electron. Dev. Lett.* **31** 1217

[15] Jessen G H, Fitch R C, Gillespie J K, Via G, Crespo A, Langley D, Denninghoff D J, Trejo M and Heller E R 2007 *IEEE Trans. Electron. Dev.* **54** 2589

[16] Vurgaftman I, Meyer J R and Ram-Mohan L R 2001 *J. Appl. Phys.* **89** 5815

[17] Farahmand M, Garetto C, Bellotti E, Brennan K F, Goano M, Ghillino E, Ghione G, Albrecht J D and Ruden P P 2001 *IEEE Trans. Electron. Dev.* **48** 535

[18] Liu J, Zhou Y G, Zhu J, Lau K M and Chen K J 2006 *IEEE Electron. Dev. Lett.* **27** 10

[19] Huq H F and Polash B 2011 *Microelectron. J.* **42** 923

[20] Bahat-Treidel E, Sidorov V, Wuerfl J and Traenkle G 2007 *Simulation of Semiconductor Processes and Devices*, September 25–27, 2007, Vienna, Austria, p. 277

[21] Ohno Y, Nakao T, Kishimoto S, Maezawa K and Mizutani T 2004 *Appl. Phys. Lett.* **84** 2184

[22] Kaddeche M, Telia A and Soltani A 2009 *International Conference on Signals, Circuits and Systems*, November 6–8, 2009, Constantine, Algeria, p. 1

[23] Sun Y and Eastman L F 2005 *Electron. Lett.* **41** 854

[24] Liu G G, Wei K, Huang J, Liu X Y and Niu J B 2011 *J. Infrared Millim. Wave* **30** 289

[25] Nakao T, Ohno Y, Kishimoto S, Maezawa K and Mizutani T 2003 *Phys. Stat. Sol.* (c) **0** 2335